ORIGINAL ARTICLE

JBMR®

Canalization Leads to Similar Whole Bone Mechanical Function at Maturity in Two Inbred Strains of Mice

Stephen H Schlecht,[1] Lauren M Smith,[2] Melissa A Ramcharan,[1] Erin MR Bigelow,[1] Bonnie T Nolan,[1] Noah J Mathis,[1] Amber Cathey,[2] Eugene Manley Jr,[3] Rajasree Menon,[4] Richard C McEachin,[4] Joseph H Nadeau,[5] and Karl J Jepsen[1]

[1]Department of Orthopaedic Surgery, University of Michigan, Ann Arbor, MI, USA
[2]School of Public Health, University of Michigan, Ann Arbor, MI, USA
[3]Department of Cell, Developmental, and Cancer Biology, Oregon Health and Science University, Portland, OR, USA
[4]Department of Computational Medicine and Bioinformatics, University of Michigan, Ann Arbor, MI, USA
[5]Pacific Northwest Diabetes Research Institute, Seattle, WA, USA

ABSTRACT

Previously, we showed that cortical mineralization is coordinately adjusted to mechanically offset external bone size differences between A/J (narrow) and C57BL/6J (wide) mouse femora to achieve whole bone strength equivalence at adulthood. The identity of the genes and their interactions that are responsible for establishing this homeostatic state (ie, canalization) remain unknown. We hypothesize that these inbred strains, whose interindividual differences in bone structure and material properties mimic that observed among humans, achieve functional homeostasis by differentially adjusting key molecular pathways regulating external bone size and mineralization throughout growth. The cortices of A/J and C57BL/6J male mouse femora were phenotyped and gene expression levels were assessed across growth (ie, ages 2, 4, 6, 8, 12, 16 weeks). A difference in total cross-sectional area ($p < 0.01$) and cortical tissue mineral density were apparent between mouse strains by age 2 weeks and maintained at adulthood ($p < 0.01$). These phenotypic dissimilarities corresponded to gene expression level differences among key regulatory pathways throughout growth. A/J mice had a 1.55- to 7.65-fold greater expression among genes inhibitory to *Wnt* pathway induction, whereas genes involved in cortical mineralization were largely upregulated 1.50- to 3.77-fold to compensate for their narrow diaphysis. Additionally, both mouse strains showed an upregulation among *Wnt* pathway antagonists corresponding to the onset of adult ambulation (ie, increased physiological loads). This contrasts with other studies showing an increase in *Wnt* pathway activation after functionally isolated, experimental in vivo loading regimens. A/J and C57BL/6J long bones provide a model to develop a systems-based approach to identify individual genes and the gene-gene interactions that contribute to trait differences between the strains while being involved in the process by which these traits are coordinately adjusted to establish similar levels of mechanical function, thus providing insight into the process of canalization. © 2017 American Society for Bone and Mineral Research.

KEY WORDS: BONE; FUNCTION; HOMEOSTASIS; CANALIZATION; *WNT/B-CATENIN* PATHWAY

Introduction

A major unresolved challenge for identifying genetic and environmental factors that contribute to skeletal health is understanding how genes work together to establish system-level function through canalization. Canalization in this context is where a population demonstrates a similar phenotype, here a mechanically competent bone, despite inherent environmental and genotype differences. This process is achieved through developmental adaptations that occur despite variation among traits that may have arisen via differing biological or environmental conditions.[1] For bone, primary system-level function includes establishing sufficient whole bone stiffness and strength during growth to resist fracturing while minimizing mass for metabolic conservation.[2,3] Targeted perturbation studies, such as gene function alterations, have provided tremendous insight into the identity of genes and molecular pathways that are involved in establishing mechanical homeostasis.[4–8] However, these studies are composed of selective decreases or increases in expression of single genes, which often lead to abnormal function,[9–12] if not an overt pathological state.[13,14] Therefore, it is difficult to determine the coordination of multiple genes in a normal physiological state from those that materialize when gene function is compromised. Likewise, genome-wide association studies have successfully located many quantitative trait loci (QTL) associated with select bone traits but have not defined how these genetic variants

Received in original form September 21, 2016; revised form January 19, 2017; accepted February 1, 2017. Accepted manuscript online February 8, 2017.
Address correspondence to: Stephen H Schlecht, PhD, Department of Orthopaedic Surgery, University of Michigan, 2148 Biomedical Sciences Research Building, 109 Zina Pitcher Place, Ann Arbor, MI 48109, USA. E-mail: sschlech@med.umich.edu
Additional Supporting Information may be found in the online version of this article.
Journal of Bone and Mineral Research, Vol. 32, No. 5, May 2017, pp 1002–1013
DOI: 10.1002/jbmr.3093

cooperate to establish whole bone mechanical function at the system level.[1,15] Thus, the ways in which genes interact to establish normal, non-pathological mechanical function is not well understood.

Our previous work has shown that in mice[16,17] and humans[18–20] phenotypic traits interact in a coordinated manner to establish a mechanically competent bone. For a given external bone size, a subset of morphological and compositional traits will predictably and coordinately adjust to offset the overall size of the bone in the interest of establishing and maintaining normal whole bone function. For example, our mouse model is composed of two inbred mouse strains that have employed different biological pathways to achieve similar whole bone strength at skeletal maturity.[21,22] A/J mice have a narrow (slender) femoral diaphysis compared with the wide (robust) femoral diaphysis of C57BL/6J (B6) mice (Fig. 1). Both strains have a similar body mass and bone length. Therefore, to offset their differences in external bone size and thus differing moment areas, they spatially distribute their cortical tissue in different ways, with A/J having a thicker cortex (ie, greater cortical area with respect to external diaphyseal diameter) compared with the thinner cortex of their B6 counterpart. Moreover, A/J mice have a more mineralized cortical matrix than B6 mice, which effectively increases the whole bone stiffness of A/J femora to functionally match the wide, more ductile femora of B6. Therefore, both mouse strains have adapted their bone structure and tissue-level material properties in different ways to maximize their skeletal stiffness and strength while simultaneously minimizing their bone mass. This phenomenon is consistent with the functional objectives observed across many species,[2,23–25] including humans.[20,26] This consistency in coordination among phenotypic traits is established early in postnatal development in mice (~2 weeks of age)[21] and humans (~2 years of age)[27] and is maintained throughout growth and into adulthood, leading us to hypothesize that this trait adjustment mechanism is canalized across species.[28] How this coordination among intermediate physical bone traits is accomplished at the genetic level remains unknown. Understanding this developmental mechanism may be clinically important for characterizing how human bone traits, which naturally vary among individuals, contribute to aging and respond to pharmacological interventions aimed at reducing fracture risk.

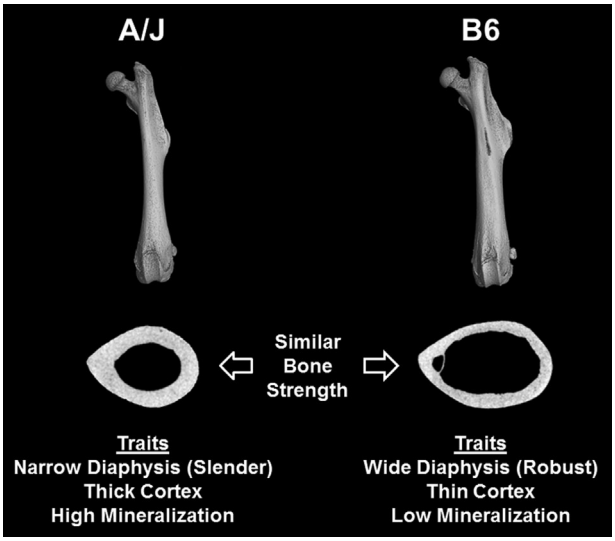

Fig. 1. Schematic highlighting the key morphological and compositional differences between male A/J and B6 mice at age 16 weeks. Note that at this age of skeletal maturity these mouse strains demonstrate equivalent bone strength. Images taken using nanoCT at an 8-μm voxel size.

Here, we use the A/J and B6 mouse model described above to begin investigating the molecular pathways between these two mouse strains whose interindividual differences in bone structure and material properties mimic that observed among humans.[29] This is a departure from a traditional targeted genetic approach, as we seek to investigate system-wide differences among unperturbed mice to investigate how genes interact to establish normal level function. This model can be used to determine how the system compensates for allelic and environmental factors that might disrupt homoeostasis, particularly those that influence the marked differences in external bone size, cortical thickness, and tissue mineralization between the two mouse strains.

We hypothesize that both mouse strains achieve a similar whole bone mechanical homeostatic state through the differential regulation of key molecular pathways contributing to the phenotypic morphological and compositional traits that differentially arise during growth. We tested this hypothesis by conducting three aims: 1) to identify which bone genes are differentially expressed between strains at multiple time points during postnatal growth, 2) to ascertain which bone-relevant pathways are differentially regulated throughout postnatal growth between strains, and 3) to determine how these gene expression profile differences between strains relate to their respective bone phenotypes at multiple time points across skeletal growth. Our goal is to understand how whole bone function is achieved at the molecular level through the differential coordination of traits, while illuminating the manner in which this mechanism may be canalized.

Materials and Methods

Before the study outlined herein, a pilot study was conducted using both male and female B6 and A/J mice at multiple time points. No statistical sex-specific difference was noted within the phenotypic or gene expression results, therefore the following study only focuses on males. Male B6 and A/J mice were acquired from The Jackson Laboratory (Bar Harbor, ME, USA) at multiple ages that span postnatal skeletal growth. Upon arrival, mice were allowed to acclimate for 1 week before euthanization. All mice were provided water and fed a standard rodent diet (Purina Rodent Chow 5001; Purina Mills, Richmond, IN, USA) ad libitum. Mice were housed at a maximum of 5 mice per cage and exposed to a 12-hour light/dark cycle. Left and right femora for phenotypic and genotypic analyses were harvested from 2-, 4-, 6-, 8-, 12-, and 16-week-old mice. These ages were chosen because it is during early postnatal growth when traits are coordinately adjusted to establish whole bone mechanical function at adulthood.[21] The University of Michigan Institutional Animal Care and Use Committee approved all mouse studies.

Phenotypic analysis

Changes in femoral diaphyseal growth were assessed at six time points throughout development (ie, 2, 4, 6, 8, 12, and 16 weeks).

Left femora were harvested from male A/J and B6 mice ($n = 10$/age/strain). Body mass (BM) was measured before euthanization. Maximum femur length (Le) was measured from the most proximal tip of the greater trochanter to the distal condyles using digital calipers (0.05 mm resolution). All femora were imaged at an 8-μm voxel size using a nanotom s (phoenix|x-ray, GE Sensing and Inspection Technologies, GmbH, Wunstorf, Germany), converted to Hounsfield units using a phantom of air, water, and hydroxyapatite (1.69 mg/cc; Gammex, Middleton, WI, USA) and reconstructed using datos|x reconstruction software (phoenix|x-ray, GE Sensing and Inspection Technologies, GmbH) as described previously.[22] Imaging parameters were varied slightly per age group to accommodate the different attenuations of the bone across groups (80 to 90 kV, 220 to 375 μA, 750 to 2000 ms, 3 to 4 average, 1 skip, 0.3 mm Al filter). These parameters were validated in house to provide the best visualization of characteristics at specific ages. From each image file, the region of interest (ROI) analyzed consisted of a 15% to 19% region of the mid-diaphysis taken just distal to the third trochanter. Each ROI was thresholded using Otsu's method.[30] ROIs were defined and variables were quantified using MicroView v2.2 Advanced Bone Analysis Application software (GE Healthcare Pre-Clinical Imaging, London, ON, Canada). Variables quantified included total cross-sectional area (Tt.Ar), cortical area (Ct.Ar), marrow area (Ma.Ar), and tissue mineral density. Cortical tissue mineral density (Ct.TMD) was derived from the mean gray value using calibration phantoms.

After computed tomography, left femora from mice aged 4 weeks and older were loaded to failure using a custom 4-point bending fixture at a displacement rate of 0.05 mm/sec (MTS 858 MiniBionix; Eden Prairie, MN, USA). Bones were kept moist with 1× phosphate-buffered saline (PBS) and tested at room temperature (RT) with the anterior surface of the femur in tension. Variables calculated from the load-deflection curves included stiffness (S), maximum load (ML), post-yield deflection (PYD), and work-to-fracture (Work), as described previously.[31,32] Two-week-old femora were not tested because of the insufficient lamellae at this growth stage to adequately perform four-point bending tests.

Gene expression analysis

Tissue preparation and RNA extraction

Gene expression profiles were obtained from RNA extracted from the femoral diaphysis of 2-, 4-, 6-, 8-, 10-, and 12-week-old male A/J and B6 mice. Sixteen-week-old mice were not used for gene expression assays because RNA concentrations yielded were drastically different between strains and, in total, substantially lower than those of the other six time points. For qPCR, 18 mice per strain and age were analyzed (6 pools of 3 mice/strain/age). For RNA sequencing, 8 mice per strain were analyzed at age 6 weeks. Mice were anesthetized with isoflurane (Piramal Healthcare, Ltd., Andhra Pradesh, India) and euthanized via cervical dislocation and a bilateral pneumothorax. For RNA extraction, the left and right femur of each animal was harvested and any adhering periosteum, muscle, tendon, and ligament were removed to detach adhering cells along the periosteal and endosteal surfaces. Next, the proximal and distal epiphyses were excised and the bone marrow was manually flushed using minimum essential medium, alpha (Gibco, ThermoFisher Scientific, Waltham, MA, USA). A histological analysis on a subset of processed bones confirmed that our tissue-harvesting protocol was effective at removing most of the adhering cells along the periosteal and endosteal surfaces (data not shown). Complete tissue preparation for each sample occurred within 6 minutes after death. Bone samples were then immediately flash frozen in liquid nitrogen and stored at –80°C.

RNA extraction was achieved by pulverizing the pair of bones in 2 mL of TRIzol (Life Technologies, Grand Island, NY, USA) using a high-speed tissue homogenizer (Model 1000; ThermoFisher Scientific). Each sample was subjected to three cycles of 20-second homogenization, placing the sample on ice between cycles to reduce thermal accumulation and subsequent RNA degradation. Total nucleic acid content was then isolated from the bone mineral and protein using 0.2 mL of 24:1 chloroform: isoamyl alcohol per 1 mL of TRIzol and subsequently centrifuged at 12,000*g* for 15 minutes at 4°C. The supernatant containing the RNA fraction was then further purified using the RNeasy Mini Kit (Qiagen, Valencia, CA, USA) and the DNA was digested on column using an RNase-Free DNase Set (Qiagen), according to the manufacturer. Total RNA was then recovered in 30 μL of RNase-free water. RNA concentration for each sample was determined using NanoDrop 2000 (ThermoFisher Scientific). RNA quality was assessed using a bioanalyzer (Model 2100; Agilent Technologies, Santa Clara, CA, USA). All samples with a 260/280 nm absorbance ratio of 1.8 or greater and an RNA integrity number greater than 8.0 were deemed to be of sufficient purity and quality for use in downstream analyses.

RNA-sequencing methodology

Whole transcriptome RNA sequencing was conducted individually on the messenger RNA (mRNA) of 8 pairs of femora from male A/J mice and 8 pairs of femora from male B6 mice at age 6 weeks. This time point was chosen because this is the age when the external size of the B6 and A/J femoral diaphysis begins its greatest divergence from one another (as reported in Results). Before library construction, each RNA sample was depleted of its ribosomal RNA (RiboGone; Clontech, Mountain View, CA, USA), according to the manufacturer. An mRNA library for each sample was subsequently prepared using the SMARTer Stranded RNA-Seq Kit (Clontech). All buffer volumes, times, and temperature settings used to construct the library were exactly as recommended in the manufacturer's protocol. Briefly, mRNA was fragmented to obtain segments of ~200 base pairs in length and converted to single-stranded cDNA that was ligated to barcode adapters. cDNA fragments were then purified using Agencourt AMPure XP magnetic beads (Beckman Coulter, Brea, CA, USA). After purification, cDNA was amplified into RNA-sequencing libraries using DNA polymerase, a universal forward PCR primer, and reverse PCR primers corresponding to the paired-end Illumina primer index. Once amplified, the RNA-sequencing library was purified using Agencourt AMPure XP magnetic beads and validated with a bioanalyzer. Upon library completion, equal volumes of stranded, bar-coded cDNA libraries generated from the left and right femora of each mouse (A/J, $n = 8$; B6, $n = 8$) were multiplexed and sequenced in quadruplicate (4 lanes of flow cell) using a HiSeq 2500 System (Illumina, San Diego, CA, USA) to obtain a minimum of 25 million base-pair reads per library.

Upon completion of sequencing, the quality of the raw reads data for each sample was checked using FastQC v1.10.1 (www.bioinformatics.bbsrc.ac.uk/projects/fastqc). Next, raw reads were aligned to the appropriate reference genomes for the A/J and B6 mouse strains using TopHat v2.0.9 and Bowtie v2.1.0. The reference genomes and the corresponding GTF files for the

A/J and B6 strains were downloaded from the Center of Genome Dynamics at The Jackson Laboratory (http://cgd.jax.org/tools/Seqnature.shtml). Alignment quality was checked using FastQC to ensure only high-quality data were used for expression quantification and differential gene expression analysis. Expression quantification at the gene level was performed using the htseq-count script embedded in HTseq. [33] This python script uses the BAM (TopHat/Bowtie output) and GTF files for generating the counts of aligned reads for each gene that overlapped its exons. The htseq-count script is designed to only count reads that mapped unambiguously to a single gene, thus reads aligned to multiple positions or overlapping with more than one gene were discarded. The counts were then used for gene-level differential expression analyses using edgeR.[34] To correct for the false discovery rate (FDR, q) p values were adjusted for multiple hypotheses testing using a Benjamini-Hochberg procedure ($q = 0.05$). Genes and transcripts that were differentially expressed between A/J and B6 mice had to not only have a q value less than or equal to 0.05 but also a fold change (Δ) (up or down) greater than or equal to 1.5. Pathway enrichment analysis was initially performed using Gene Ontology.[35] Ingenuity Pathway Analysis software (Qiagen) was then used to identify significantly differentially expressed canonical pathways and functional groupings of genes. Pathway analyses were performed using a right-tailed Fisher's exact test to generate a p value representing the probability that differentially expressed genes placed in a given pathway were not due to random chance and a Benjamini-Hochberg correction was applied to account for multiple comparisons ($q = 0.05$).

RNA sequencing was confirmed and validated using a custom TaqMan microfluidic array card (Applied Biosystems, Foster City, CA, USA) that encoded for 45 *Wnt* pathway-related genes and three endogenous controls using qPCR (Model 7900HT RT-PCR; Applied Biosystems) (Supplemental Table S1). As reported in the results below, an enrichment analysis using Gene Ontology of the RNA-sequencing data showed the canonical *Wnt* pathway to be significantly differentially expressed ($\geq$2-fold) between the A/J and B6 mouse femora.

qPCR analysis

Gene expression changes in both B6 and A/J mouse strains across growth were tracked using cDNA generated from 2-, 4-, 6-, 8-, 10-, and 12-week-old male mice. RNA samples were combined into 6 pools per strain and age (3 samples per pool) to yield 200 ng of RNA per pool. Reverse transcription was performed on each pooled sample using qScript cDNA SuperMix (Quanta Biosciences, Gaithersburg, MD, USA) and was run in a C1000 Thermal Cycler (Bio-Rad Laboratories, Hercules, CA, USA) according to the manufacturer. Each cDNA sample was then combined with TaqMan Gene Expression Master Mix (Applied Biosystems) and loaded into custom 384-well microfluidic array cards containing 45 unique primers related to the canonical and non-canonical *Wnt* pathways and three endogenous control primers (Supplemental Table S1). Each card allowed for 8-pooled samples to be run simultaneously. Cards were then centrifuged at 4°C (Legend XTR with custom TaqMan array card bucket; Sorvall, Waltham, MA, USA) and sealed. Cards were run in accordance with the manufacturer's recommendations.

After the generation of the amplification plots, the baseline and threshold settings were adjusted to obtain an accurate threshold cycle (C_T) that was the same for both strains at each given age. A comparative C_T method ($\Delta\Delta C_T$) was used to calculate fold-change expression levels by normalizing the data to an endogenous reference.[36] Because of the specificity, sensitivity, and amplification efficiency of the TaqMan assays,[37] fold changes (up or down) of 1.5 or greater that were identified as being statistically significant ($p < 0.05$) via a paired t test met our criteria for denoting differences in gene expression levels between the two strains.

Protein analysis

Left and right femora of B6 and A/J 6-week-old male mice ($n = 10$/strain) were harvested in the same manner as described for RNA preparation. Whole cell extracts (lysates) were obtained by homogenizing both femora of two mice (5 pools/strain) in 50 mM Tris-base, 150 mM sodium chloride, 2 mM ethylene glycol tetraacetic acid, 10 mM sodium pyrophosphate decahydrate, and 10% nonyl phenoxypolyethoxylethanol for 30 seconds. Equal protein lysate concentrations (13 μg per pool) were separated on 4% stacking gels and 12% SDS-PAGE gels (150V, 90 minutes) and transferred to nitrocellulose membranes (100V, 60 minutes). Membranes were blocked for 1 hour at RT with 5% bovine serum albumin (BSA) diluted in Tris-buffered saline containing 0.05% Tween 20 (TBS-T). After blocking, the membranes were incubated overnight at 4°C with a rabbit polyclonal anti-sclerostin antibody (sc130258, Santa Cruz Biotechnology, Dallas, TX, USA) diluted at 1:200 in 5% BSA. Membranes were then washed in TBS-T and incubated in a goat anti-rabbit immunoglobulin-G horseradish peroxidase-conjugated secondary antibody (sc2004, Santa Cruz Biotechnology) diluted at 1:20,000 in 5% BSA for 1 hour at RT. After rinsing in TBS-T, the blots were developed on Fuji HR-T X-ray film (Fujifilm Medical Systems, Stamford, CT, USA) using SuperSignal West Femto Maximum Sensitivity Substrate (ThermoFisher Scientific).

Statistical analysis

All data were analyzed using Minitab v16 (State College, PA, USA) and Prism v6 (GraphPad Software, La Jolla, CA, USA). A Shapiro-Wilk test confirmed that the data were normally distributed. To test for phenotypic differences between strains at each age, a general linear model (GLM) analysis of variance (ANOVA) was employed. A GLM was used to adjust all traits relative to BM for each age separately, which is a known covariate to these traits. Additionally, Tt.Ar was included as a covariate to Ct.Ar, Ma.Ar, and Ct.TMD because these traits vary relative to external bone size. Significance was taken at a p value equal to or less than 0.05. An analysis of covariance (ANCOVA) was employed to test for significance in growth trajectories between mouse strains for Tt.Ar and Ct.TMD because these traits have previously been shown to have the greatest divergence between strains. This was done by plotting each trait against the logarithm of age to linearize the data, followed by a comparison of the slopes and y-intercepts to determine differences in phenotypes across growth. Using a Bonferroni correction to adjust for multiple comparisons, significance of the phenotypic data between strains across ages was based on an alpha level of 0.008. Effect sizes were reported as Cohen's d. These were calculated as the difference between the means between strains for any given trait divided by the pooled standard deviation of those means. Gene expression level differences between mice strains were quantitatively assessed as described in the Gene Expression Analysis subsection of Materials and Methods.

Western blot data was analyzed using a paired *t* test with significance taken at a *p* value equal to or less than 0.05.

Results

Femoral phenotypes for both B6 and A/J mice were largely established by age 2 weeks

The unadjusted and adjusted means along with the standard deviations of all pertinent phenotype data are listed in Supplemental Table S2. By age 2 weeks, a significant 33% difference in external bone size (ie, Tt.Ar) between A/J and B6 mice was established and maintained throughout growth to age 16 weeks (A/J: 0.68–1.33 mm^2; B6: 1.01–2.04 mm^2; effect size = 4.39–6.77; $p < 0.001$, GLM ANOVA; slope: $p < 0.0001$, ANCOVA) (Fig. 2*A*). Periosteal expansion of the femoral diaphysis was largely complete in both strains by age 8 weeks. Ma.Ar increased between ages 2 and 4 weeks within both strains, with A/J mice showing significantly less marrow space into adulthood compared with B6 (A/J: 0.57–0.97 mm^2; B6: 0.64–1.04 mm^2; effect size = 1.23–3.71; $p < 0.07$–0.001, GLM ANOVA) (Fig. 2*C*). Ct.Ar relative to external diaphyseal size was significantly higher in A/J femora compared with B6 femora across growth (ages 2 to 16 weeks), which explains their thicker cortex (A/J: 0.26–0.91 mm^2; B6: 0.20–0.85 mm^2; effect size = 1.23–3.71; $p < 0.07$–0.0001, GLM ANOVA) (Fig. 2*B*). For A/J to accommodate a narrower diaphysis while not drastically altering their absolute volume of tissue, they significantly increased their Ct.TMD by age 8 weeks (A/J: 1321 ± 32.61 mg/cc; B6: 1257 ± 31.28 mg/cc; effect size = 2.00; $p = 0.004$, GLM ANOVA; y-intercept: $p < 0.0001$, ANCOVA) (Fig. 2*D*). This tissue-level adjustment partially contributed to a 10% significant difference in whole bone stiffness (A/J: 215.4 ± 23.9 N/mm; B6: 195.0 ± 23.4 N/mm; effect size = 0.86; $p = 0.02$, GLM ANOVA) (Fig. 3*A*) but only a 3% non-significant difference in ML at age 16 weeks (A/J: 28.6 ± 2.5 N; B6: 27.7 ± 2.4 N; effect size = 0.35; $p = 0.33$, GLM ANOVA) (Fig. 3*B*). However, these adjustments in cortical mineralization, and in turn whole bone stiffness, in A/J femora throughout growth came at a mechanical cost, resulting in a more brittle bone as evidenced by the 62% to 77% significant difference in post-yield displacement between strains throughout growth (A/J: 0.12–0.24 mm; B6: 0.33–0.90 mm; effect size = 2.13–7.28; $p < 0.001$, GLM ANOVA) (Fig. 3*C*). This lower post-yield displacement largely contributed to the 41% to 58% significantly less work-to-fracture in A/J during growth (AJ: 4.92–7.33 Nmm; B6: 8.35–14.21 Nmm; effect size = 1.48–4.62; $p < 0.005$, GLM ANOVA) (Fig. 3*D*). This phenotypic analysis thus confirms that the primary morphological and compositional differences between B6 and A/J femora were external bone size and tissue mineral density and that these differences are apparent as early as age 2 weeks.

Femoral gene expression profiles significantly differed between B6 and A/J mice

RNA sequencing of the femoral cortical matrices of 6-week-old A/J and B6 mice yielded 4290 genes that showed significant differential expression between strains ($q \leq 0.05$, fold ≥ 1.5). From these genes, we identified 9 canonical pathways that largely encompass the morphological (ie, external bone size) and compositional (ie, cortical matrix mineralization) development of bone (Supplemental Table S3). The canonical (*β-catenin*) and non-canonical (PCP, Ca^{+}) *Wnt* pathways were integral to many of the identified pathways and the majority of the recognized genes encompassing these 9 pathways demonstrated at least a 1.5-fold increased expression in A/J mice relative to B6 mice. The enrichments of greatest interest, selected using Gene Ontology, are listed in Table 1. These enrichments were all upregulated in A/J mice relative to B6 and qualitatively correlated well with the phenotypic differences observed between these mice at skeletal maturity (ie, Tt.Ar and Ct.TMD).

The canonical *Wnt* pathway, which is instrumental in driving mesenchymal stem cells toward the osteoblastic lineage, demonstrated a twofold enrichment between mouse strains. Ingenuity Pathway Analysis identified 45 of 165 known *Wnt* pathway-related genes in our bone samples. All but six of these genes showed greater expression in A/J relative to B6. Using knockout/knockdown models, others have identified several of these 45 genes to be antagonistic to the canonical *Wnt* pathway.

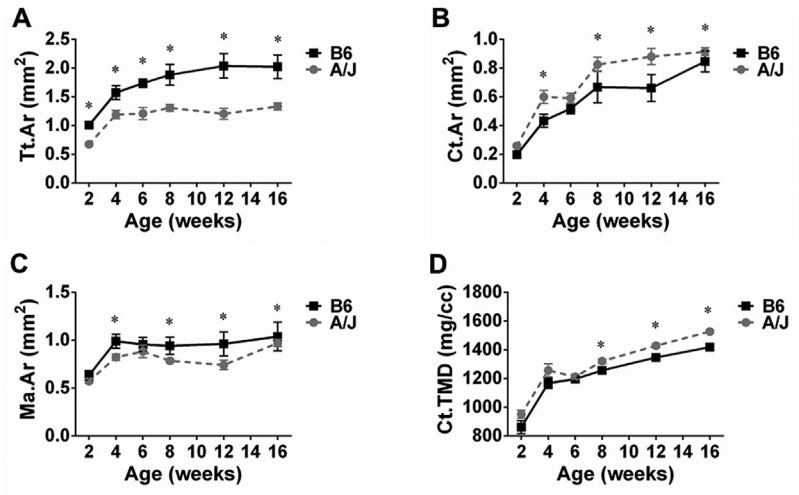

Fig. 2. Mean and standard deviations of bone morphological and compositional traits across multiple time points during growth and development after adjusting for body mass (*A*) or both body mass and total area (*B–D*). (*A*) Total area (Tt.Ar); (*B*) cortical (Ct.Ar); (*C*) marrow area (Ma.Ar); (*D*) cortical tissue mineral density (Ct.TMD). * Denotes significant differences between B6 and A/J mice at the $p < 0.05$ alpha level.

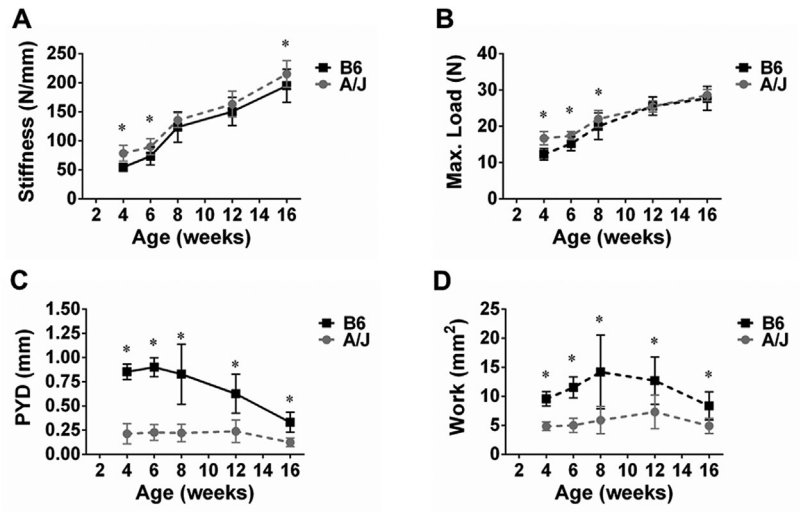

Fig. 3. Mean and standard deviations of mechanical four-point bending data across multiple time points during bone growth and development after adjusting for body mass. (*A*) Stiffness; (*B*) maximum load; (*C*) post-yield displacement (PYD); (*D*) work-to-fracture (work). *Denotes significant differences between B6 and A/J mice at the $p < 0.05$ alpha level.

When looking at the total net accumulated perturbation (a gene's measured fold change combined with the accumulated perturbation transmitted from any upstream genes) of each of the 45 genes identified in our data set, the greater antagonism of the canonical *Wnt* pathway in A/J through disruption of *Wnt* ligand signaling and binding translated downstream into a reduction in *Dvl* and *β-catenin*, as well as reduced *Tcf/Lef* transcription. Fig. 4 demonstrates this outcome on the *Wnt/β-catenin* KEGG pathway. These RNA sequencing results were validated by our qPCR analysis of *Wnt* pathway-related genes (below).

An additional outcome of the Gene Ontology and Ingenuity Pathway analyses was the identification of several genes that collectively play a substantial role in bone mineralization ($-\log(p) = 3.54\text{e-}03$ and 1.86e-09, respectively). The expression levels of the majority of these genes were elevated in A/J femora relative to B6 femora. Of particular note was that A/J showed greater expression among genes recently discovered to comprise the acidic serine aspartate-rich *Mepe*-associated motif (ASARM) bone-renal mineral pathway, which includes *Phex* (fold $\Delta = 2.45$), *Dmp1* (fold $\Delta = 2.19$), and *Mepe* (fold $\Delta = 2.86$). Complementing the greater expression of these genes in A/J femora was the elevated gene expression levels of many other genes known to play a functional role in bone mineralization (Supplemental Table S4), relative to B6. The greater expression level of these genes in A/J femora qualitatively correlates with the higher Ct.TMD values observed in the phenotypic analysis of these mice.

Expression levels of Wnt pathway antagonist genes were higher in A/J femora, but expression levels shifted at a greater magnitude in B6 mice throughout growth

Mapping the canonical and non-canonical *Wnt* pathway-related gene expression profiles across growth using the custom microfluidic array cards highlighted several differences between A/J and B6 mice. Throughout growth, many of the 45 genes assayed that are involved in either the induction or inhibition of canonical *Wnt* pathway signaling demonstrated elevated expression in A/J mice relative to B6 mice (Table 2). Genes that were elevated in expression among A/J mice that suggest pathway induction included *Wnt10b*, *Ctnnb1*, *Lef1*, and *Tcf7*, whereas genes that suggest pathway inhibition because of their elevated expression in A/J mice included *Wif1*, *Sost*, *Dkk1*, *Dkk2*, *Sfrp1*, and *Sfrp4*. Despite this juxtaposition in higher expression levels among genes that either promote or suppress canonical *Wnt* pathway signaling within A/J mice relative to B6 mice, the inhibitors collectively exhibited greater expression levels than their downstream targets involved in an activated pathway (Fig. 5). This suggested that A/J mice have some degree of sustained *Wnt* pathway inhibition throughout growth with respect to B6 mice, similar to the results obtained from the RNA sequencing of 6-week-old mice. *Sost* showed the greatest difference in expression levels among these inhibitory genes, which was confirmed at the protein level (ie, sclerostin) in 6-week-old mice via Western blots. A/J had a significantly higher concentration ($p = 0.03$) of sclerostin compared with B6 (Fig. 6).

Table 1. Enrichment of Genes Playing Key Roles in Bone Development Identified Using Gene Ontology's Panther Classification System

Functional enrichments	No. of genes	−log (*p* value)	Fold enrichment
Collagen fibril organization	21	5.70e-03	3.66
Regulation of osteoblast differentiation	46	1.33e-04	2.58
Regulation of bone mineralization	31	3.54e-03	2.85
Skeletal system morphogenesis	71	1.58e-04	2.08
Regulation of canonical *Wnt* signaling pathway	53	2.57e-02	2.00

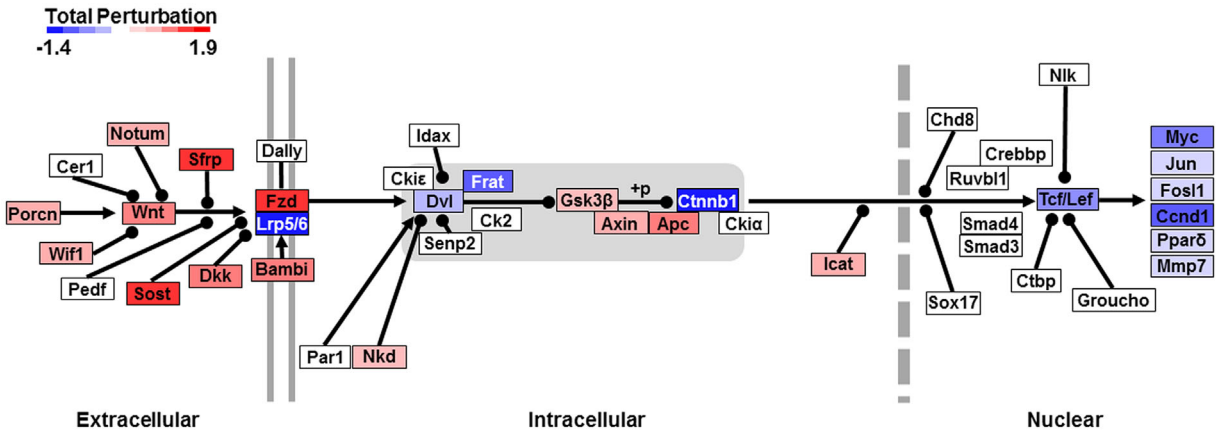

Fig. 4. Schematic of the canonical *Wnt* pathway modeled after the KEGG diagram, highlighting the total perturbation of genes (a gene's measured fold change combined with the accumulated perturbation transmitted from any upstream genes) identified via RNA sequencing of B6 and A/J mouse femora at age 6 weeks. Color scale denotes the perturbation level of A/J femoral genes relative to those of B6. Blue denotes a decrease in a gene's functional role and red denotes an increase in a gene's functional role.

To determine the magnitude in which expression profiles of genes involved in the *Wnt* pathway changed across growth between A/J and B6 mice, the $\Delta\Delta C_T$ values for each gene analyzed were plotted as a function of age by normalizing the values at each time point to the $\Delta\Delta C_T$ values at age 2 weeks (ie, their baseline expression level). Normalization of gene expression levels within both strains to their respective 2-week age revealed that although A/J mice have greater overall gene expression with regard to genes involved in the *Wnt* pathway across growth relative to B6 mice, B6 mice actually showed greater shifts in gene expression among genes compared with A/J mice (Fig. 7). The gene demonstrating the greatest expression level change at all time points across growth in both mouse strains was *Sost*. From their baseline fold change ratio of 1 at age 2 weeks, A/J showed a maximum 5-fold change in expression during growth, whereas B6 showed a maximum 7.5-fold change in expression.

Discussion

We tested the hypothesis that A/J and B6 mice achieve a mechanical homeostatic state through the differential regulation of key molecular pathways that correspond with their phenotypic differences in external femoral bone size and mineralization. RNA sequencing and qPCR analyses were conducted on cortical bone of the femoral diaphysis. Analyses of femoral bone RNA throughout growth found significantly different gene expression profiles present between A/J and B6 mice as early as age 2 weeks. This timeframe corresponded to an age when a difference in Tt.Ar and Ct.TMD was already apparent between A/J and B6 male mouse femora, suggesting that the differing biological pathways employed to achieve bone mechanical competence is canalized. Many of the genes identified from RNA sequencing reflect bone development, with expression levels of these genes being largely greater for A/J mice relative to B6 mice. Collectively, the genes identified comprise pathways involved in bone homeostasis and mineralization.[7] The canonical *Wnt* pathway, which many have shown to drive osteoblastic differentiation and thus an increase in bone formation (see Baron and Kneissel[7] for a review), was found to play an integral role in many of the enriched pathways resulting from the RNA sequencing of these 6-week-old mice. An assessment of key genes encompassing this pathway across multiple time points during growth found gene expression levels that were primarily expressed at a higher level among A/J males relative to B6 males. Because A/J mice show a narrower femoral diaphysis, albeit with a relatively thicker, more mineralized cortex, the elevated expression levels among several genes known to either inhibit *Wnt* signaling or increase cortical mineralization at age 6 weeks suggested a compensatory mechanism may be in place to adjust tissue-level strength relative to external bone size. This hypothesis is bolstered with the finding of greater expression levels among genes involved in the ASARM bone-renal pathway, which has been shown to play a regulatory role in mineralization, phosphate regulation, soft-tissue calcification, osteoclastogenesis, and mechanotransduction.[38]

Also of interest from the phenotype and gene expression data is that despite relatively greater gene expression levels among *Wnt* pathway inhibitors in A/J mice, gene expression levels, after being normalized to the 2-week time point (ie, baseline expression level), tended to increase during growth at a greater magnitude (ie, fold) among B6 mice compared with that of A/J mice. Thus, there are strain and age-specific gene expression differences. This shift in expression levels among *Wnt* pathway inhibitory genes may provide a mechanism where the periosteal expansion of B6 diaphyses, which are already wide relative to A/J, is held in check, particularly during the rapid growth phase occurring between ages 4 and 8 weeks. Additionally, the lower expression levels of genes involved in cortical mineralization among B6 mice at age 6 weeks complements the phenotypic data concerning their lower Ct.TMD relative to their A/J counterparts, who show increased signaling for mineralizing activity to offset their narrow diaphysis.

Collectively, the gene expression profile data support the dichotomy in external bone size and whole bone stiffness observed phenotypically throughout growth between A/J and B6 mice. By differentially inducing or inhibiting molecular pathways known to play a role in bone homeostasis, it would appear that A/J and B6 mice are able to maintain an intricate

Table 2. Gene Expression Differences of *Wnt* Pathway-Related Genes Using Custom Array Cards

	Age 2 weeks		Age 4 weeks		Age 6 weeks		Age 8 weeks		Age 12 weeks	
Gene	Fold Δ		Fold Δ		Fold Δ		Fold Δ		Fold Δ	
Wnt1	**2.66**	↑	**1.35**		**3.08**	↑	**3.18**	↑	**3.34**	↑
Wnt5a	**1.78**	↑	0.93		**2.06**	↑	**2.65**	↑	**3.32**	↑
Wnt6	**0.47**	↓	0.52		0.54		0.77		**2.70**	↑
Wnt7b	**1.62**	↑	**0.57**	↓	**1.53**	↑	1.98		**5.48**	↑
Wnt10a	1.31		0.82		1.34		**2.06**	↑	5.36	
Wnt10b	**1.84**	↑	0.88		**2.01**	↑	**1.99**	↑	**3.71**	↑
Fzd1	1.28		0.88		**1.88**	↑	**1.72**	↑	**2.72**	↑
Fzd2	**1.79**	↑	1.22		**3.75**	↑	**4.40**	↑	**7.09**	↑
Fzd6	1.07		0.87		1.33		**1.80**	↑	**3.58**	↑
Fzd8	**1.68**	↑	0.95		**1.86**	↑	**2.94**	↑	**3.50**	↑
Lrp4	1.23		0.79		**1.74**	↑	**2.10**	↑	**3.29**	↑
Lrp5	1.18		0.83		**2.50**	↑	**1.82**	↑	3.88	
Lrp6	1.10		0.96		**1.76**	↑	1.56		**2.40**	↑
Dvl1	**1.45**		0.97		**1.78**	↑	**1.75**	↑	**2.31**	↑
Axin1	**1.25**		0.87		1.25		1.26		**1.60**	↑
Axin2	1.28		0.99		**2.51**	↑	**2.34**	↑	**4.45**	↑
Apc	1.12		0.98		**1.68**	↑	**1.74**	↑	**3.34**	↑
Gsk3β	1.07		0.92		**1.45**		**1.49**		**2.64**	↑
Ctnnb1	1.28		0.85		**1.84**	↑	**1.90**	↑	**3.04**	↑
Lef1	0.85		1.00		**1.78**	↑	**1.77**	↑	**3.48**	↑
Tcf7	**1.29**		1.04		**2.38**	↑	**2.70**	↑	**2.81**	↑
Sfrp1	0.97		1.19		**1.44**		**2.02**	↑	**2.05**	↑
Sfrp4	**1.55**		0.89		**1.67**	↑	**1.55**	↑	**2.43**	↑
Wif1	**0.73**		**0.74**		**1.98**	↑	**2.67**	↑	**3.77**	↑
Sost	**7.65**	↑	**1.70**	↑	**5.91**	↑	**5.14**	↑	**4.66**	↑
Dkk1	**2.69**	↑	1.18		**3.70**	↑	**2.93**	↑	**4.94**	↑
Dkk2	**2.13**	↑	1.13		**2.98**	↑	**3.12**	↑	**3.69**	↑
Notch1	0.95		0.60		0.94		0.90		1.16	
Sostdc1	1.22		**2.21**	↑	1.63		7.75		**6.15**	↑
Cepba	1.29		1.23		**1.48**		**1.96**	↑	**1.78**	↑
Pparγ	0.78		1.13		1.00		1.33		1.67	↑
Msx2	0.45	↓	0.52	↓	1.90	↑	1.40		1.81	
Tnfrsf11b	1.62	↑	0.88		2.52	↑	2.41	↑	2.88	↑
Tnfsf11	1.05		0.87		2.00	↑	3.25	↑	2.34	↑
Runx2	1.34		0.98		1.91	↑	2.20	↑	3.70	↑
Sp7	1.70	↑	1.20		2.95	↑	2.85	↑	3.73	↑
Calca	0.71		0.57		2.94		1.63		—	
Twist1	1.07		0.48	↓	1.08		1.54		2.30	↑
Wisp1	2.00	↑	1.05		2.70	↑	2.62	↑	6.13	↑

Fold changes represent differential gene expression levels in A/J mice relative to B6 mice. Directional arrows indicate up- or downregulation of all genes showing a 1.5 or greater fold change (up or down), regardless of p value. Bold denotes significance at the $p < 0.05$ alpha level of A/J gene expression relative to B6 for each time point, regardless of fold change.

balance between bone mass and strength in the interest of achieving a mechanically and metabolically functional bone at adulthood. This outcome was not unexpected because Currey and Alexander[2] hypothesized years ago that the ultimate goal of bone is to achieve mechanical and metabolic function through a balance of stiffness and mass. The phenotypic and gene expression profiles of mice comprising our model support this hypothesis, with A/J and B6 mice potentially reaching the same functional endpoint through the differential regulation of genes encompassing the *Wnt* pathway and functional mineralization network involved in achieving a homeostatic state between external bone size (ie, mass) and cortical mineralization (ie, tissue stiffness).

Our assessment of gene expression within the *Wnt* pathway during growth provided new insight into the role of *Sost*, and other inhibitors of the *Wnt* pathway (eg, *Dkk1*, *Dkk2*, *Sfrp1*, *Sfrp4*, etc.), on the development of external bone size. *Sost* encodes the protein sclerostin, a major antagonist to the *Wnt* pathway in bone, which effectively blocks *Wnt* ligands from binding to the *Lrp5/6* receptors thereby inhibiting downstream signaling.[39,40] Outcomes of targeted knockout studies[41–44] and studies suppressing sclerostin expression using monoclonal antibodies[45–48] have consistently shown that activation of the *Wnt* pathway is associated with increased periosteal expansion and marrow infilling. In our study, A/J mice demonstrated a narrow femoral diaphysis with a 2- to 8-fold higher *Sost* expression throughout growth relative to B6 femora. Although periosteal expansion is largely completed by age 8 weeks in A/J femoral diaphyses, they continue to deposit bone endosteally to offset their narrow diaphysis. This continuation of marrow infilling once periosteal expansion ceases is important as it enables A/J mice to achieve a near similar Ct.Ar as B6 mice in the interest of constructing a mechanically competent bone that is comparable to the whole bone strength and stiffness achieved by B6 upon skeletal maturity. This outcome suggests that the diaphyseal phenotype observed in A/J femora is not solely dependent on *Sost* expression but most likely depends on interactions among many genes. Moreover, the roles *Sost* and other *Wnt* pathway inhibitors play throughout growth may differ depending on the age of the mouse, as others have previously shown.[49] Overall, the outcome of the gene expression analysis narrows the focus of alleles and suggests that allelic differences between A/J and B6 mice lead to suppression of the entire *Wnt* pathway in A/J mice, while bolstering their functional competence with a greater expression level among genes integral to an increase in cortical mineralization. To further explore how mechanical function is established during growth, it would be beneficial to expand analyses to naturally perturbed mouse strains (eg, recombinant inbred, chromosome substitution, collaborative cross, heterogeneous stock). These strains are largely non-pathologic and can minimize the interpretive complications that may arise from the presence of flanking genes in targeted gene perturbation models.[50]

Although a comparison of gene expression differences between A/J and B6 was consistent with expectations for the role of *Wnt* signaling in regulating external bone size, a comparison of gene expression across growth was inconsistent with previous studies. The 2- to 7.5-fold increase in *Sost* expression between ages 2 and 4 weeks for A/J and B6 mice was in juxtaposition to the findings of others who reported a decrease in *Sost* expression among mice subjected to artificially applied loads.[41–44,51] This was unexpected because it has been reported that mice transition into full adult ambulatory activities between these time points,[52] which presumably places greater physiologically relevant, weight-bearing mechanical loads on the skeletal system. The discrepancy between these outcomes could result from differences in the ages (eg, 10 to 20 weeks of age) and skeletal elements (eg, ulnae, tibias, fibulae) of the animals investigated in prior studies,[41,42,44] or from the assumption that tissue strains would increase during the initial phases of ambulation. Moreover, differences between our findings and those of others may indicate that genes and the proteins they encode potentially play different roles depending on whether

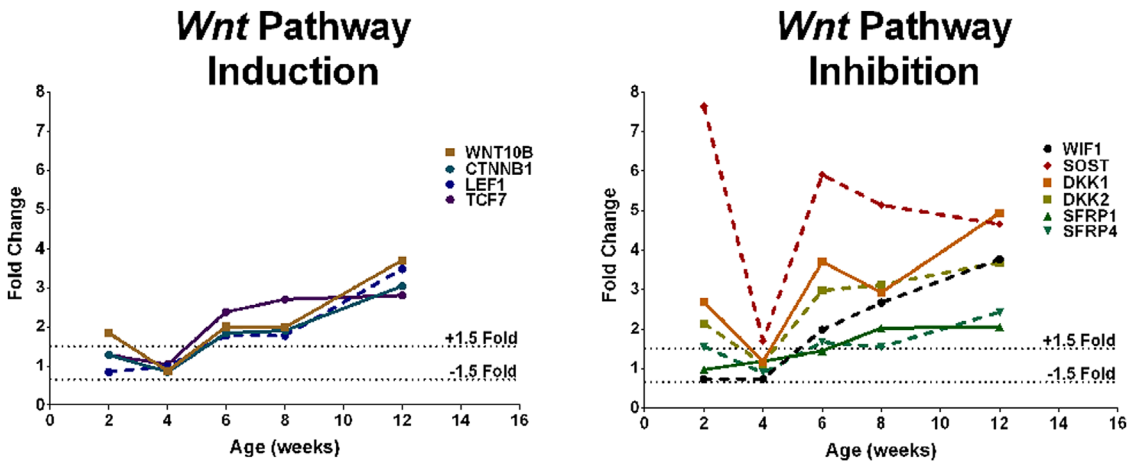

Fig. 5. Canonical *Wnt* gene expression changes in A/J relative to B6 mice throughout growth in (*A*) key pathway inducers and (*B*) key pathway inhibitors via custom array cards. Note the collectively greater expression of inhibitory genes of the pathway relative to those that promote induction.

they are acting in a physiological or pathophysiological state.[53] However, despite the incongruity between studies, the increase in *Sost* expression in both A/J and B6 mice throughout growth is consistent with the increase in serum sclerostin observed across growth for human boys and girls,[54] although the association between *SOST* expression and serum sclerostin levels is not well understood.[55] Finding a qualitative correlation between an increase among *Sost* and the transition to full ambulation among mice that have different phenotypic trait sets suggests the relationship between this key *Wnt* pathway antagonist and bone formation is more complex than has been previously shown among mice that are selectively perturbed. Based on previous findings, one would expect that as total diaphyseal area (ie, bone formation) increases by $\sim$0.5 mm^2, *Sost* expression would decrease to allow *β-catenin* to accumulate in the cytoplasm and translocate to the nucleus to induce *Tcf/Lef* transcription factors to drive mesenchymal stem cells toward the osteoblastic lineage. Therefore, it remains unclear as to what role *Sost* may be playing during the shift to full ambulation. Further investigation into this relationship is required.

One limitation of this study is that only the gene expression differences of cells remaining in the cortical matrix after the removal of the bone marrow and musculotendinous tissue were examined. Presumably, bone cells present along the periosteal and endosteal surfaces also play an important mediatory role in external bone size and mineralization. Future work will need to independently assay the fibrous periosteum and bone marrow to determine the role these tissues have in regulating the distribution and composition of bone in space with regards to the differing diaphyseal phenotypes present in the current model. For example, others have shown periostin, an extracellular matrix protein that in bone is localized to the periosteum and expressed by the osteoblastic lineage, to promote collagen cross-linking via enhancement of lysyl oxidase activation.[51] Additionally, assays of the associated bone marrow could inform on whether signaling pathways responsible for osteoblastic and osteoclastic differentiation is differentially induced or inhibited between strains. Another limitation of this study is that we did not determine whether *Sost* is differentially expressed across the periosteal, intracortical, and endosteal envelopes to stimulate a localized adaptive bone formation response, which may explain why periosteal bone formation, but not endosteal infilling, was impeded in A/J mice.

In conclusion, the current study has confirmed that there are inherent gene expression profile differences between the cortical diaphysis of two inbred mouse strains that have different phenotypic trait sets yet similar whole bone function by skeletal maturity. Therefore, it would appear that the genotypic background of these mice contributes to their phenotypic outcome in a canalized manner, as hypothesized. A/J mice have a narrow femoral diaphysis that is highly mineralized, which coincides with their gene expression profile, suggesting that the *Wnt* pathway is being inhibited to some degree throughout growth while the ASARM bone–renal pathway and the greater mineralization functional network is being activated. Importantly, though the *Wnt*

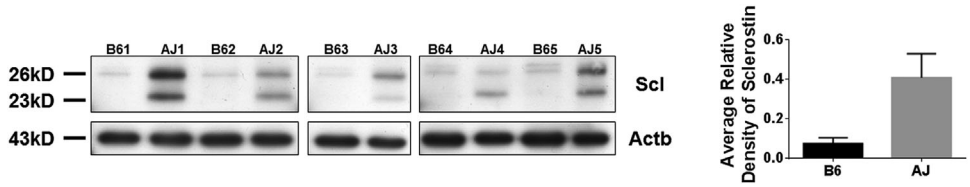

Fig. 6. Sclerostin protein expression in 6-week-old B6 and A/J femora via Western blot. The upper band at 26 kD may be a result of glycosylation, as sclerostin is believed to have N-glycosylation sites.[57] The right panel shows the relative difference in sclerostin protein expression based on gray value band intensity at the 23 kD molecular weight.

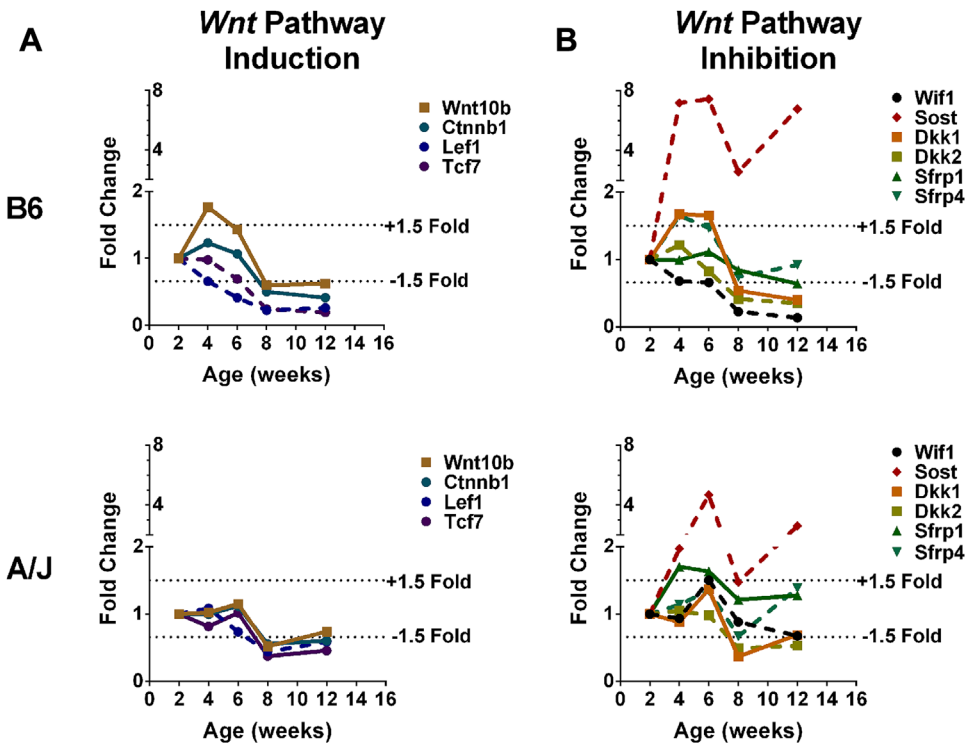

Fig. 7. Canonical *Wnt* pathway gene expression changes in (*A*) key pathway inducers and (*B*) key pathway inhibitors throughout growth. Fold changes reported are those after normalization of the data to the 2-week time point. Note the greater magnitude of change for *Sost* in B6 mice compared with A/J mice.

pathway appears to be inhibited in A/J femora, this does not translate to a meaningful difference in absolute Ct.Ar relative to B6 femora. In addition to this finding, the dichotomy between high expression level changes among antagonists to the *Wnt* pathway in both strains during a period of greater physiological loads (ie, adult ambulatory activity) and the decrease in these same antagonists upon the application of artificial loads, as reported by others, suggests that the role these genes play in developing and maintaining bone homeostasis is more complex than previously thought. To increase our understanding of the role genetic and environmental backgrounds have in establishing function during growth, future work should focus on teasing apart the functional networks responsible for coordinating external bone size, bone mass, and mineralization so that the traits together lead to a bone with sufficient stiffness and strength to be functional under physiological loads. Identifying alleles that may contribute to the physiological differences observed within an animal model that mimics the natural variation among complex trait sets known to contribute to the mechanical competence of bone in humans is of primary importance. This requires a more systems-based approach, rather than a reductionist one, to detect interactions both between genes and between genes and their environment, all of which contribute to the development of whole bone function.[1,15] An integrative approach that takes advantage of mouse strains developed from natural genetic recombinatory activities over several generations of random breeding may allow us to better understand the underlying functional networks responsible for the establishment of whole bone functional competence.[56]

Disclosures

All authors state that they have no conflicts of interest.

Acknowledgments

The authors thank the University of Michigan DNA Sequencing and Bioinformatics Cores for their assistance and guidance in RNA sequencing. We thank Drs Andrea Alford and Ernestina Schipani for comments and suggestions regarding the study design, and Charles Roehm and Anita Reddy for their technical support.

This work was supported by grants from the U.S. National Institutes of Health (KJJ: R01AR44927 and S10RR026336; SHS: T32 DE007057).

Authors' roles: Study design: KJJ, JHN, SHS, LMS, and EM. Mouse colony management: BTN and LMS. Data collection: SHS, LMS, EMRB, NM, and AC. Data analysis: SHS, LMS, RM, RCM, and KJJ. Data interpretation: SHS, KJJ, JHN, LMS, MR, RM, and RCM. Manuscript preparation: SHS, LMS, KJJ, JHN, RM, and MR. Manuscript approval: SHS, LMS, MR, EMRB, BTN, NM, AC, EM, RM, RCM, JHN, and KJJ.

References

1. Nadeau JH, Burrage LC, Restivo J, Pao YH, Churchill G, Hoit BD. Pleiotropy, homeostasis, and functional networks based on assays of cardiovascular traits in genetically randomized populations. Genome Res. 2003;13:2082–91.
2. Currey JD, Alexander RM. The thickness of the walls of tubular bones. J Zool. 1985;206:453–68.

3. Seeman E. Bone quality: the material and structural basis of bone strength. J Bone Miner Metabol. 2008;26:1–8.
4. Cao X, Chen D. The BMP signaling and in vivo bone formation. Gene. 2005;357:1–8.
5. Edwards JR, Mundy GR. Advances in osteoclast biology: old findings and new insights from mouse models. Nat Rev Rheumatol. 2011;7:235–43.
6. Long F. Building strong bones: molecular regulation of the osteoblast lineage. Nat Rev Mol Cell Biol. 2012;13:27–38.
7. Baron R, Kneissel M. WNT signaling in bone homeostasis and disease: from human mutations to treatments. Nat Med. 2013;19:179–92.
8. Lieben L, Carmeliet G. The delicate balance between vitamin D, calcium and bone homeostasis: lessons learned from intestinal- and osteocyte-specific VDR null mice. J Steroid Biochem Mol Biol. 2013;136:102–6.
9. Luo G, Ducy P, McKee MD, et al. Spontaneous calcification of arteries and cartilage in mice lacking matrix GLA protein. Nature. 1997;386:78–80.
10. Delany AM, Amling M, Priemel M, Howe C, Baron R, Canalis E. Osteopenia and decreased bone formation in osteonectin-deficient mice. J Clin Invest. 2000;105:915–23.
11. Hankenson KD, Bain SD, Kyriakides TR, Smith EA, Goldstein SA, Bornstein P. Increased marrow-derived osteoprogenitor cells and endosteal bone formation in mice lacking thrombospondin 2. J Bone Miner Res. 2000;15:851–62.
12. Ameye L, Aria D, Jepsen K, Oldberg A, Xu T, Young MF. Abnormal collagen fibrils in tendons of biglycan/fibromodulin-deficient mice lead to gait impairment, ectopic ossification, and osteoarthritis. FASEB J. 2002;16:673–80.
13. Schwarzbauer JE, Spencer CS. The Caenorhabditis elegans homologue of the extracellular calcium binding protein SPARC/osteonectin affects nematode body morphology and mobility. Mol Biol Cell. 1993;4:941–52.
14. Komori T, Yagi H, Nomura S, et al. Targeted disruption of Cbfa1 results in a complete lack of bone formation owing to maturational arrest of osteoblasts. Cell. 1997;89:755–64.
15. Farber CR. Systems-level analysis of genome-wide association data. G3 Genes Genome Genet. 2013;3:119–29.
16. Jepsen KJ, Akkus OJ, Majeska RJ, Nadeau JH. Hierarchical relationships between bone traits and mechanical properties in inbred mice. Mamm Genome. 2003;14:97–104.
17. Jepsen KJ, Hu B, Tommasini SM, et al. Genetic randomization reveals functional relationships among morphologic and tissue-quality traits that contribute to bone strength and fragility. Mamm Genome. 2007;18:492–507.
18. Jepsen KJ, Centi A, Duarte GF, et al. Biological constraints that limit compensation of a common skeletal trait variant lead to inequivalence of tibial function among healthy young adults. J Bone Miner Res. 2011;26:2872–85.
19. Schlecht SH, Jepsen KJ. Functional integration of skeletal traits: an intraskeletal assessment of bone size, mineralization, and volume covariance. Bone. 2013;56:127–38.
20. Schlecht SH, Bigelow EMR, Jepsen KJ. Mapping the natural variation in whole bone stiffness and strength across skeletal sites. Bone. 2014;67:15–22.
21. Price C, Herman BC, Lufkin T, Goldman HM, Jepsen KJ. Genetic variation in bone growth patterns defines adult mouse bone fragility. J Bone Miner Res. 2005;20:1983–91.
22. Smith L, Bigelow EMR, Nolan BT, Faillace ME, Nadeau JH, Jepsen KJ. Genetic perturbations that impair functional trait interactions lead to reduced bone strength and increased fragility in mice. Bone. 2014;67:130–8.
23. Alexander RM. *Optima for animals. Revised ed*. Princeton, NJ: Princeton University Press 1996. 176 p.
24. Papadimitriou HM, Swartz SM, Kunz TH. Ontogenetic and anatomic variation in mineralization of the wing skeleton of the Mexican free-tailed bat, Tadarida brasiliensis. J Zool. 1996;240:411–26.
25. Dumont ER. Bone density and the lightweight skeletons of birds. Proc Royal Soc B: Biol Sci. 2010;277:2193–8.
26. Jepsen KJ, Hu B, Tommasini SM, et al. Phenotypic integration of skeletal traits during growth buffers genetic variants affecting the slenderness of femora in inbred mouse strains. Mamm Genome. 2009;20:21–33.
27. Pandey N, Bhola S, Goldstone A, et al. Interindividual variation in functionally adapted trait sets is established during postnatal growth and predictable based on bone robustness. J Bone Miner Res. 2009;24:1969–80.
28. Waddington CH. Canalization of development and the inheritance of acquired charcteristics. Nature. 1942;14:563–5.
29. Jepsen KJ, Bigelow EMR, Schlecht SH. Women build long bones with less cortical mass relative to body size and bone size compared with men. Clin Orthop Relat Res. 2015;473(8):2530–9.
30. Otsu N. A threshold selection method from gray-level histograms. IEEE Trans Syst Man Cybern. 1979;SMC-9:62–6.
31. Jepsen K, Goldstein S, Kuhn J, Schaffler M, Bonadio J. Type-I collagen mutation compromises the post-yield behavior of Mov13 long bone. J Orthop Res. 1996;14:493–9.
32. Jepsen KJ, Pennington DE, Lee Y-L., Warman M, Nadeau J. Bone brittleness varies with genetic background in A/J and C57BL/6J inbred mice. J Bone Miner Res. 2001;16:1854–62.
33. Anders S, Pyl P, Huber W. HTSeq—a Python framework to work with high-throughput sequencing data. Bioinformatics. 2014;31:166–9.
34. Huang DW, Sherman BT, Lempicki RA. Bioinformatics enrichment tools: paths towards the comprehensive functional analysis of large gene lists. Nucl Acids Res. 2009;37:1–13.
35. Ashburner M, Ball C, Blake J, et al. Gene ontology: a tool for the unification of biology. Nat Genet. 2000;25:25–9.
36. Livak KJ, Schmittgen TD. Analysis of relative gene expression data using real-time quantitative PCR and the 2 delta delta Ct method. Methods. 2001;25:402–8.
37. ThermoFisher Scientific. Gene expression assay performance guaranteed with the TaqMan assays qPCR guarantee program. 2015. Applied Biosystems White Paper: docs.appliedbiosystems.com/pebiodocs/088754.pdf.
38. Rowe PS. Regulation of bone-renal mineral and energy metabolism: the PHEX, FGF23, DMP1, MEPE ASARM pathway. Crit Rev Eukaryot Gene Expr. 2012;22:61–86.
39. Krishnan V, Bryant HU, MacDougald OA. Regulation of bone mass by Wnt signaling. J Clin Invest. 2006;116:1202–9.
40. Duan P, Bonewald LF. The role of the wnt/β-catenin signaling pathway in formation and maintenance of bone and teeth. Intern J Biochem Cell Biol. 2016;77:23–9.
41. Robling AG, Niziolek PJ, Baldridge LA, et al. Mechanical stimulation of bone in vivo reduces osteocyte expression of sost/sclerostin. J Biol Chem. 2008;283:5866–75.
42. Moustafa A, Sugiyama T, Saxon LK, et al. The mouse fibula as a suitable bone for study of functional adaptation to mechanical loading. Bone. 2009;44:930–5.
43. Tu X, Rhee Y, Condon KW, et al. Sost downregulation and local Wnt signaling are required for the osteogenic response to mechanical loading. Bone. 2012;50:209–17.
44. Morse A, McDonald MM, Kelly NH, et al. Mechanical load increases in bone formation via a sclerostin-independent pathway. J Bone Miner Res. 2014;29:2456–67.
45. Padhi D, Jang G, Stouch B, Fang L, Posvar E. Single-dose, placebo-controlled, randomized study of AMG 785, a sclerostin monoclonal antibody. J Bone Miner Res. 2011;26:19–26.
46. McColm J, Hu L, Womack T, Tang CC, Chiang AY. Single- and multiple-dose randomized studies of blosozumab, a monoclonal antibody against sclerostin, in healthy postmenopausal women. J Bone Miner Res. 2014;29:935–43.
47. McClung MR, Grauer A, Boonen S, et al. Romosozumab in postmenopausal women with low bone mass. N Engl J Med. 2014;370:412–20.
48. Padhi D, Allison M, Kivitz AJ, et al. Multiple doses of sclerostin antibody romosozumab in healthy men and postmenopausal women with low bone mass: a randomized, double-blind, placebo-controlled study. J Clin Pharmacol. 2014;54:168–78.

49. Sinder BP, Lloyd WR, Salemi JD, et al. Effect of anti-sclerostin therapy and osteogenesis imperfecta on tissue-level properties in growing and adult mice while controlling for tissue age. Bone. 2016;84:222–9.
50. Wolfer DP, Crusio WE, Lipp H-P. Knockout mice: simple solutions to the problems of genetic background and flanking genes. Trends Neurosci. 2002;25:336–40.
51. Bonnet N, Standley KN, Bianchi EN, et al. The matricellular protein periostin is required for Sost inhibition and the anabolic response to mechanical loading and physical activity. J Biol Chem. 2009;284:35939–50.
52. Fox WM. Reflex-ontogeny and behavioural development of the mouse. Anim Behav. 1965;13:234–41.
53. Tonsor SJ, Alonso-Blanco C, Koornneef M. Gene function beyond the single trait: natural variation, gene effects, and evolutionary ecology in Arabidopsis thaliana. Plant Cell Environ. 2005;28:2–20.
54. Kirmani S, Amin S, McCready LK, et al. Sclerostin levels during growth in children. Osteop Intern. 2012;23:1123–30.
55. Clarke BL, Drake MT. Clinical utility of serum sclerostin measurements. Bonekey Rep. 2013;361:1–7.
56. Farber CR, van Nas A, Ghazalpour A, et al. An integrative approach to identify candidate genes regulating BMD: combining linkage, gene expression, and association. J Bone Miner Res. 2009;24:106–16.
57. Kusu N, Laurikkala J, Imanshi M, et al. Sclerostin is a novel secreted osteoclast-derived bone morphogenetic protein antagonist with unique ligand specificity. J Biol Chem. 2003;278:24113–7.